JOURNAL OF SOLID STATE CHEMISTRY 94, 404–417 (1991)

# The Crystal Chemistry Underlying Ferroelectricity in $Bi_4Ti_3O_{12}$, $Bi_3TiNbO_9$, and $Bi_2WO_6$

R. L. WITHERS, J. G. THOMPSON, AND A. D. RAE*

*Research School of Chemistry, Australian National University, G.P.O. Box 4, Canberra, A.C.T., 2601, Australia; and*
**School of Chemistry, University of New South Wales, P.O. Box 1, Kensington, New South Wales 2033, Australia*

Received March 4, 1991; in revised form June 4, 1991

The recent rerefinements of the crystal structures of $Bi_4Ti_3O_{12}$, $Bi_3TiNbO_9$, and $Bi_2WO_6$ differ substantially from earlier reported structure refinements. A comparison of the major structural distortions present in each of these materials is presented and the main structural cause of ferroelectricity (in $Bi_4Ti_3O_{12}$ and $Bi_3TiNbO_9$) is shown to be the *a*-axis displacement of Bi atoms in the perovskite A sites with respect to the chains of $TiO_6$ octahedra and not the perovskite B atoms moving toward an octahedral edge. By using a modulated structure approach, the driving force for this displacement and other structural features can be simply understood in terms of the need to satisfy bond valence requirements. © 1991 Academic Press, Inc.

## 1. Introduction

Within the family of so-called Aurivillius phases (*1, 2*), there exists a large number of displacive ferroelectrics (*3, 4*) whose room temperature structures can be described in terms of relatively small amplitude, displacive perturbations away from a high symmetry, prototype, parent structure (space group symmetry $I4/mmm$, $a_p = b_p \approx 3.85$ Å, p = perovskite). This nonpolar, prototype, parent structure consists of perovskite-like $A_{n-1}B_nO_{3n+1}$ slabs regularly interleaved with $Bi_2O_2$ layers and is usually presumed to correspond to the crystal structure of these materials above the high temperature phase transition which occurs at their respective Curie temperatures.

To date, the Bravais lattices of the known ferroelectric Aurivillius phases have almost invariably been reported (*5*) as having a doubled $\sqrt{2}a_p \times \sqrt{2}a_p$ basal plane cell ($\mathbf{a} = \mathbf{a}_p + \mathbf{b}_p$, $\mathbf{b} = -\mathbf{a}_p + \mathbf{b}_p$) and by *A*-centering (for *n* even) and *B*-centering (for *n* odd). The infinite wavelength strain wave accompanying the displacive modulations responsible for this expansion of the basal plane cell leads to a slight orthorhombic distortion of the new basal plane cell (i.e. $a \neq b$) and formally transforms the $I4/mmm$ ($a_p = b_p \approx 3.85$ Å, *c*) prototype parent structure to an $Fmmm$ ($a \approx b \approx 3.85\sqrt{2}$ Å, *c*) underlying "average" structure. This we will henceforth refer to as the parent structure (see Fig. 1).

The structural deviation of these displacive ferroelectrics from this underlying, nonpolar, $Fmmm$ parent structure can then be Fourier decomposed into displacive modulations characterized by the mod-

0022-4596/91 $3.00

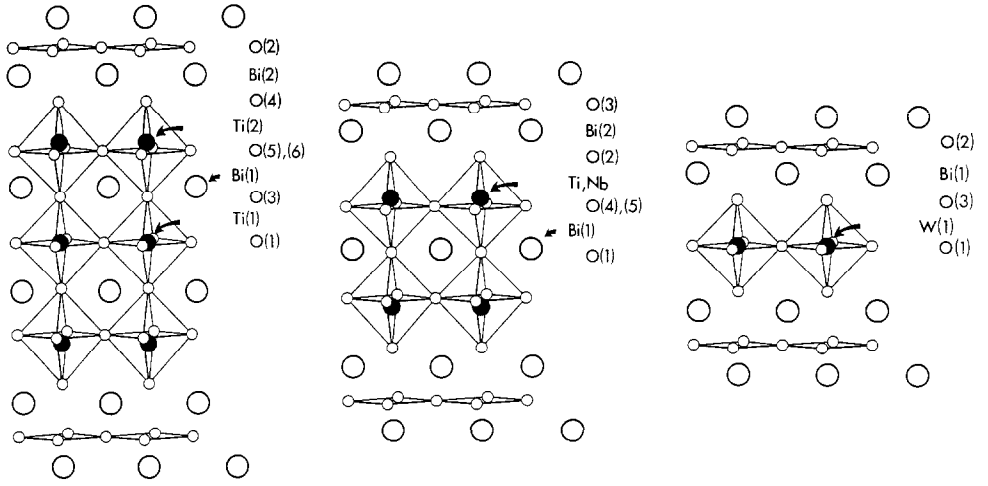


FIG. 1. A perspective drawing, approximately down ⟨110⟩, of the undistorted *Fmmm* parent structures of $Bi_4Ti_3O_{12}$, $Bi_3TiNbO_9$, and $Bi_2WO_6$. Only atoms between 1/4*c* and 3/4*c* are shown.

ulation wave vectors $\mathbf{q} = \mathbf{a}^*$ and $\mathbf{q} = 0$ (for a resultant *A*-centered lattice), $\mathbf{q} = \mathbf{b}^*$ and $\mathbf{q} = 0$ (for a resultant *B*-centered lattice) or $\mathbf{q} = \mathbf{a}^*$, $\mathbf{q} = \mathbf{b}^*$, $\mathbf{q} = \mathbf{c}^*$, and $\mathbf{q} = 0$ (for a resultant primitive lattice) (*6–8*). There are eight irreducible representations associated with the little cogroup (*9*) of each of these modulation wave vectors (see Table I). Displacive modes characterized by a particular modulation wave vector (i.e., $\mathbf{q} = \mathbf{a}^*$, $\mathbf{q} = \mathbf{b}^*$, $\mathbf{q} = \mathbf{c}^*$, or $\mathbf{q} = 0$) and by one of these irreducible representations give rise to atomic displacement patterns with the specific space group symmetries listed in Table I. Knowledge of the resultant space group symmetry of a particular ferroelectric Aurivillius phase is equivalent to knowledge of the possible displacive modes present. Thus, for example, the *B2cb* (equivalent to *B2ab*) space group symmetry previously reported as characteristic of *n* odd ferroelectric Aurivillius

TABLE I

THE IRREDUCIBLE REPRESENTATIONS OF *Fmmm* ASSOCIATED WITH THE $\mathbf{k} = \mathbf{a}^*, \mathbf{k} = \mathbf{b}^*, \mathbf{k} = \mathbf{c}^*, \mathbf{k} = 0$ POINTS OF THE BRILLOUIN ZONE AND THEIR EFFECTIVE SPACE GROUP LABELS (SPACE GROUP CORRESPONDING TO THE SYMMETRY OPERATION WITH CHARACTERS OF +1). ONLY THE SYMMETRY ELEMENTS WITH A ZERO TRANSLATIONAL COMPONENT ARE LISTED.

| | 1 | $2_x$ | $2_y$ | $2_z$ | −1 | $m_x$ | $m_y$ | $m_z$ | $\mathbf{k} = \mathbf{a}^*$ | $\mathbf{k} = \mathbf{b}^*$ | $\mathbf{k} = \mathbf{c}^*$ | $\mathbf{k} = 0$ |
|---|---|---|---|---|---|---|---|---|---|---|---|---|
| $X_1$ | +1 | +1 | +1 | +1 | +1 | +1 | +1 | +1 | *Ammm* | *Bmmm* | *Cmmm* | *Fmmm* |
| $X_2$ | +1 | +1 | −1 | −1 | +1 | +1 | −1 | −1 | *Amaa* | *Bmab* | *Cmca* | *F*2/*m*11 |
| $X_3$ | +1 | −1 | −1 | +1 | +1 | −1 | −1 | +1 | *Abam* | *Bbam* | *Cccm* | *F*112/*m* |
| $X_4$ | +1 | −1 | +1 | −1 | +1 | −1 | +1 | −1 | *Abma* | *Bbmb* | *Ccma* | *F*12/*m*1 |
| $X_5$ | +1 | +1 | +1 | +1 | −1 | −1 | −1 | −1 | *Abaa* | *Bbab* | *Ccca* | *F*222 |
| $X_6$ | +1 | +1 | −1 | −1 | −1 | −1 | +1 | +1 | *Abmm* | *Bbmm* | *Ccmm* | *F*2*mm* |
| $X_7$ | +1 | −1 | −1 | +1 | −1 | +1 | +1 | −1 | *Amma* | *Bmmb* | *Cmma* | *Fmm*2 |
| $X_8$ | +1 | −1 | +1 | −1 | −1 | +1 | −1 | +1 | *Amam* | *Bmam* | *Cmcm* | *Fm*2*m* |

phases is compatible with displacive modes of *Bmab*, *Bbab*, *F2mm*, and *Fmmm* symmetry.

Recently we have rerefined the crystal structures of $Bi_4Ti_3O_{12}$, $Bi_3TiNbO_9$, and $Bi_2WO_6$ in such terms (*6–8*) and found substantial differences from earlier reported structure refinements—both with respect to previously reported space group symmetries (and hence with respect to the number and type of displacive modulations present) and also with respect to the internal nature of the *F2mm* displacive modulation responsible for spontaneous polarization along the a-axis. The space group symmetry of $Bi_2WO_6$, for example, was found to be $P2_1ab$—a subgroup of the previously reported *B2cb* space group symmetry. Similarly, by contrast with the previously reported structure refinements (*10–12*), the *F2mm a*-axis shifts of the atoms making up the perovskite $BO_6$ octahedra were all found to have the same sign in each of the three rerefinements. Comparison of the equivalent displacive modulations in each of the three structures shows a remarkable similarity in behavior. This casts serious doubts on the previously reported structural basis for ferroelectricity in this family of compounds (*5*). The purpose of this paper is twofold: first, to present a structural comparison of the major displacive modulations present in each of these three structures and, second, to use bond length–bond valence formalism (*14–16*) to provide an insight into the crystal chemical reasons underlying these structural distortions and, hence, ferroelectricity in $Bi_4Ti_3O_{12}$, $Bi_3TiNbO_9$, and $Bi_2WO_6$.

## 2. Comparison of the Major Structural Distortions Present in $Bi_4Ti_3O_{12}$, $Bi_3TiNbO_9$ and $Bi_2WO_6$

Analysis of these three rerefined crystal structures shows that the octahedral shape of the oxygen framework in the perovskite slabs of the parent structure remains intact to a very good approximation and hence can be usefully employed to describe the major structural distortions taking place. The space group symmetries and major displacive modes present in each of these three crystal structures are given in Table II. The induced minor displacive components (see Table 3 of Ref. (*8*)) all have very small amplitudes and can be neglected for the purposes of this paper. There are three major types of displacement modes always present in the rerefined structures. They can be described as follows:

(i) The *F2mm* mode, directly responsible for the observed macroscopic spontaneous polarization along the **a** direction (see Fig.

TABLE II

MAJOR AND MINOR DISPLACIVE MODES FOR THE COMMENSURATELY MODULATED STRUCTURES OF $Bi_4Ti_3O_{12}$, $Bi_3TiNbO_9$ AND $Bi_2WO_6$

| *n* | Compound | Space group | Major components | | Minor components | |
|---|---|---|---|---|---|---|
| 3 | $Bi_4Ti_3O_{12}$ | *B*1*a*1 | *F2mm*<br>*Bbab* | *Bmab*<br>*Bbam* | *Fmm*2<br>*Bmam* | *F*12/*m*1 |
| 2 | $Bi_3TiNbO_9$ | $A2_1am$ | *F2mm*<br>*Amam* | *Abam* | | |
| 1 | $Bi_2WO_6$ | $P2_1ab$ | *F2mm*<br>*Abam* | *Bmab* | *Bbab*<br>*Ccma* | *Amam*<br>(*Cmma*) |

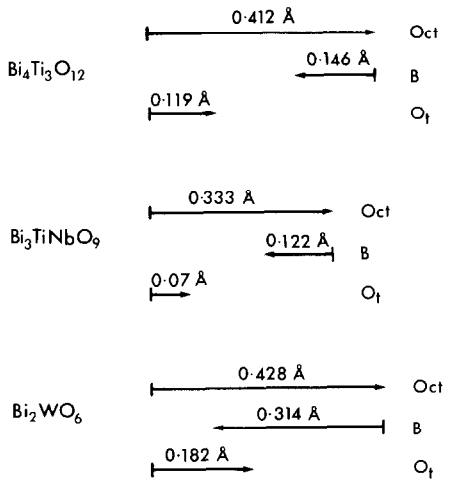


FIG. 2. Shows a schematic representation of the *F2mm* atomic displacement pattern. The arrows represent shifts relative to stationary [001] chains of Bi atoms. The upper arrow (labeled Oct) corresponds to the averaged shift along **a** of the $B_nO_{3n+1}$ part of the perovskite slabs. The middle arrow (labeled B) corresponds to the averaged motion back in the opposite direction of the perovskite *B* cation with respect to the surrounding oxygen octahedral framework. The lower arrow (labeled $O_t$; t for tetrahedral) corresponds to the averaged motion along the **a** direction of the oxygen ions within the $Bi_2O_2$ layer. This *F2mm* mode gives rise to the large component of spontaneous polarization along **a**.

3 of (*6*), Fig. 4 of (*7*), and Fig. 6 of (*8*)), can be described in terms of three sets of atomic shifts relative to virtually stationary [001] chains of Bi cations. First, a more or less rigid shift along the **a** direction of the $B_nO_{3n+1}$ part of the perovskite slabs. Second, motion back in the opposite direction of the perovskite *B* cations with respect to their surrounding oxygen octahedral framework. Third, a rigid motion along the **a** direction of the oxygen ions within the $Bi_2O_2$ layer. These shifts are schematically illustrated in Fig. 2. While the "$Bi_2O_2$ layer" oxygen motion in one sense could be thought of as being part of the oxygen octahedral framework, the magnitude of the shifts involved is always substantially less than the magnitude of the shifts of the other oxygen atoms. Hence they have been separated out. Note that the motion of the B cation with respect to its surrounding $O_6$ octahedron is approximately twice as large for $Bi_2WO_6$ as for $Bi_4Ti_3O_{12}$ and $Bi_3TiNbO_9$.

The relative contributions of these three types of motion to the calculated macroscopic spontaneous polarization in each case are given in Table III. The macroscopic spontaneous polarization along **a**, $P_x$, was calculated assuming point charges ($q_i = +3$ for Bi, $+4.5$ for the composite (Ti,Nb) ion, $+6$ for W, and $-2$ for oxygen) and using the formula

$$P_x = \sum_i \frac{q_i \Delta x_i}{V},$$

where the summation over $i$ is over all the ions contained in the underlying, nonpolar, *Fmmm* parent structure (volume $V$) and where $q_i$, $\Delta x_i$ represent the charge and displacement along **a** of these ions. Note that only the *F2mm* mode can make a contribution to $P_x$. Note that the motion of the octahedral perovskite *B* cations within their surrounding $O_6$ octahedra is now, in contrast to the previously reported structure refinements (*5*), no longer the overwhelmingly dominant contributor to the calculated

TABLE III

THE RELATIVE CONTRIBUTION TO THE CALCULATED SPONTANEOUS POLARIZATION (IN UNITS OF $\mu C/cm^2$) OF THE THREE TYPES OF *F2mm* MOTION

| Compound | Oct[a] | *B*[b] | $O_t$[c] |
|---|---|---|---|
| $Bi_4Ti_3O_{12}$ | 22.1 | 11.7 | 3.2 |
| $Bi_3TiNbO_9$ | 14.7 | 9.7 | 2.5 |
| $Bi_2WO_6$ | 11.4 | 25.1 | 9.7 |

[a] The contribution due to the averaged shift along **a** of the $B_nO_{3n+1}$ part of the perovskite slabs.

[b] The contribution due to the averaged motion back in the opposite direction of the perovskite *B* cation with respect to its surrounding oxygen octahedral framework.

[c] The contribution due to the averaged motion along the **a** direction of the oxygen ions within the $Bi_2O_2$ layer.

spontaneous polarization even in the case of $Bi_2WO_6$—although its relative contribution to the calculated spontaneous polarization does appear to systematically increase as $n$ decreases. The large change in the internal nature, i.e., the motion of the atoms relative to each other, of the *F*2*mm* displacive modulations occasioned by these rerefinements leads to a similarly large change in the relative contributions of the above three components to the calculated spontaneous polarization and clearly requires a reevaluation of the crystal chemistry underlying the existence of ferroelectricity in these materials. In the case of the previous structure refinement of $Bi_3TiNbO_9$ (*12*), the shift of the octahedral perovskite *B* cations within their surrounding $O_6$ octahedra contributes some 87% of the calculated spontaneous polarization.

(ii) The *Bmab* mode for $n$ odd and the *Amam* mode for $n$ even consists of alternating rotations of octahedra about axes parallel to **a** (for "to scale" drawings see Fig. 2 of (*6*), Fig. 5 of (*7*), and Fig. 5 of (*8*)) as schematically illustrated in Fig. 3. Note that the oxygen atoms making up the perovskite $O_6$ octathedra are constrained to move in either the **b** or the **c** directions for such modes and, hence, such octahedral rotation is also automatically accompanied by octahedral expansion. The average octahedral rotation angles are quite large and correspond to $+8.6°$, $-10.6°$, and $+8.6°$ for the three octahedra in the perovskite slab of $Bi_4Ti_3O_{12}$ (an average rotation angle of $\sim 9.3°$), $\sim 8.9°$ for $Bi_3TiNbO_9$, and $\sim 10.3°$ for $Bi_2WO_6$. Hence there is a remarkable degree of similarity in the magnitude of this type of structural distortion for each of the three rerefinements.

(iii) The *Bbab* and *Bbam* modes for $n = 3$, the *Abam* mode for $n = 2$, and the *Abam* and *Bbam* modes for $n = 1$ consist of $BO_6$ octahedral rotation modes about axes parallel to **c** (for "to scale" drawings see Fig. 4 of Ref. (*6*), Fig. 6 of Ref. (*7*), and Fig. 7 of Ref. (*8*)) as schematically illustrated in Fig. 4. Note that the equatorial oxygen atoms

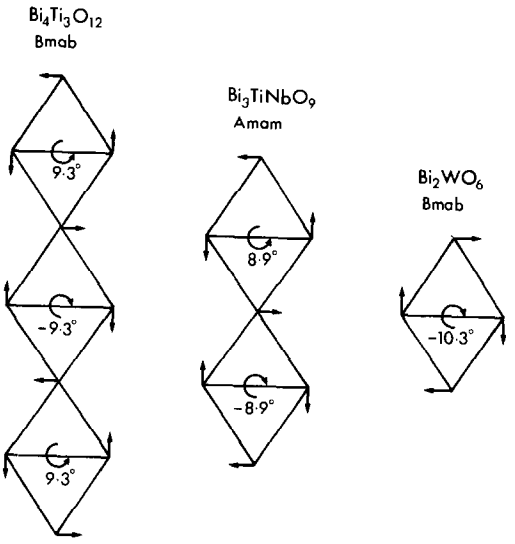


FIG. 3. Shows a schematic representation of the atomic displacements associated with the octahedral rotation around **a** modes (*Bmab* for $n$ odd and *Amam* for $n$ even). The oxygen atom shifts are exaggerated by a factor of three.

making up the perovskite $O_6$ octahedra are constrained to move in either the **a** + **b** or the **a** − **b** directions for such modes and, hence, such octahedral rotation is also automatically accompanied by an expansion of the octahedral size in the lateral dimension perpendicular to **c**. Note also that such modes cause the least disruption to the apical oxygens of the perovskite slab as well as to the $Bi_2O_2$ layer and, hence, might be expected to be the modes most susceptible to losing phase coherence across $Bi_2O_2$ layers.

For $n$ odd, the *b* glide perpendicular to **c** of the *Bbab* mode constrains the central $BO_6$ octahedron of each perovskite slab not to rotate and the outer $BO_6$ octahedra to rotate in the opposite sense. In the case of $Bi_4Ti_3O_{12}$, these angular rotation angles are $+7.5°$, $0°$, and $-7.5°$. In the case of $Bi_2WO_6$, the only $BO_6$ octahedra per perovskite slab (the central one) is similarly constrained not to rotate. Thus, in order for the central $BO_6$ octahedra to be allowed to rotate about the

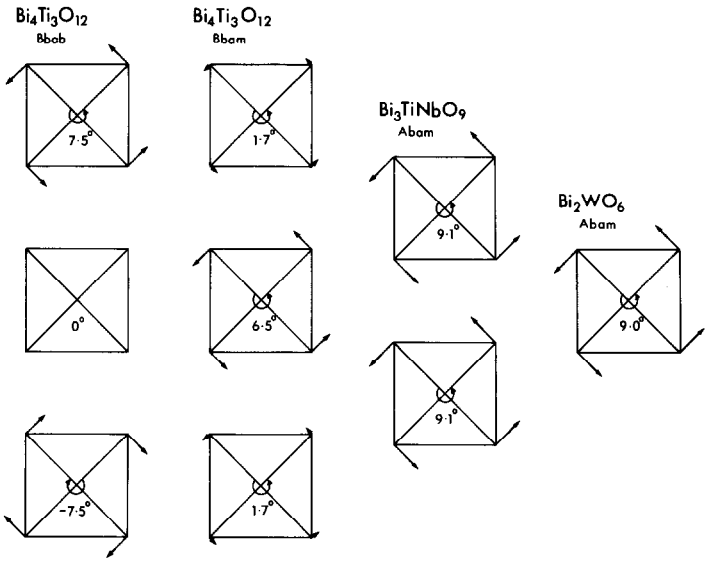


FIG. 4. Shows a schematic representation of the atomic displacements associated with the octahedral rotation around **c** modes (*Bbab* and *Bbam* for $n = 3$, *Abam* for $n = 2$ and $n = 1$). Again the oxygen atom shifts are exaggerated by a factor of three.

*c*-axis, the space group symmetry of *n* odd Aurivillius phases must in every case be lowered from the previously reported *B*2*cb* space group symmetry. The appropriate symmetry lowering modes have either *Bbam* or *Abam* symmetry, the difference being associated with the way this mode stacks across $Bi_2O_2$ layers perpendicular to **c**.

Within a perovskite slab of $Bi_4Ti_3O_{12}$, the *m* plane perpendicular to **c** now allows the central octahedron to rotate and constrains the two outer octahedra to rotate in the same sense. In the case of $Bi_4Ti_3O_{12}$, the observed symmetry lowering mode has *Bbam* symmetry and the observed rotation angles are 1.7°, 6.5°, and 1.7°. In the case of $Bi_2WO_6$, both symmetry lowering modes are observed in the form of a fine scale coherent intergrowth (see Fig. 3 of Rae *et al.* (*8*)) of two distinct modulated variants—the majority variant with $P2_1ab$ symmetry corresponding to the *Abam* symmetry lowering mode and the other with the same symmetry as $Bi_4Ti_3O_{12}$, i.e., $B1a1$, corresponding to the *Bbam* mode symmetry lowering option. The rotation angle for the majority *Abam* mode is ~9.0°.

For *n* even, the *m* plane perpendicular to **c** of the *Abam* mode constrains mirror-related octahedra to rotate in the same sense and hence there is no need for an additional symmetry lowering mode as in the case of *n* odd Aurivillius phases. In the case of $Bi_3TiNbO_9$, the magnitude of this octahedral rotation angle around **c** is ~9.1°. Again, there is a remarkable degree of similarity in the magnitude of this sort of structural distortion for each of the three rerefined crystal structures.

## 3. The Application of the Bond Valence Method

Various approaches to the understanding of bond lengths in crystals have been used with the most widespread approach being based upon the concept of ionic radius. There are, however, severe difficulties associated with this ionic radii approach which are largely overcome in the bond valence method.

In this latter approach, the relationship between the length of a bond ($r^{ij}$) and its valence ($s^{ij}$) is written in the form:

$s^{ij} = \exp[(r_0^{ij} - r^{ij})/B]$, where $r_0^{ij}$ and $B$ are empirical parameters which can be refined via use of the Inorganic Crystal Structure Database (ICSD). The apparent valence (AV) of atom $i$, $V_i'$, is then obtained as a sum over all the neighboring bond valences i.e., $V_i' = \Sigma_j s^{ij}$. Brown and Altermatt (*13*) have refined the parameters $r_0^{ij}$ and $B$ for over 750 atom pairs and listed the 141 most accurately determined values for $r_0^{ij}$. They find empirically that $B$ can be set to a constant—namely, 0.37 Å.

### 3.1 $Bi_4Ti_3O_{12}$—Detailed Analysis

Using Brown and Altermatt's values of $r_0^{ij}$ for $Bi^{3+}$–$O^{2}$-bonds and $Ti^{4+}$–$O^{2-}$ bonds, in conjunction with the fourier decomposition of the rerefined crystal structure (see Tables 6 and 9 of (*6*)), we can now attempt to systematically investigate the crystal chemistry of $Bi_4Ti_3O_{12}$. Table IV lists the calculated apparent valences and the root mean square deviation of these AVs ($\Sigma V = ((^1/N \Sigma (AV_n - V_n)^2)^{1/2}$, where $N$ is the number of atoms in the asymmetric unit) from their expected values for the *Fmmm* parent structure on its own (see under the column headed PAR) as well as in combination with various of the observed displacive modes (see Figs. 2, 3, and 4 of (*6*)). AVs and $\Sigma V$s are also listed for the final refined structure (see under the column headed 1.8%), for an $R = 2.7\%$ structure corresponding to a false minimum in the structure refinement (see under the column headed 2.7%), and

TABLE IV

CALCULATED APPARENT VALENCES FOR $Bi_4Ti_3O_{12}$[a]

| Atom | Par | *F2mm* | *Bmab* | *Bbab* | *Bbam* | *Fmm2* | 2 modes | 3 modes | 4 modes | 5 modes | 1.8% | 2.7% | Dorrian |
|---|---|---|---|---|---|---|---|---|---|---|---|---|---|
| Bi(1) | 2.36 | 2.89 | 2.63 | 2.50 | 2.39 | 2.40 | 3.14 | 3.12 | 3.14 | 3.18 | 3.21 | 3.17 | 2.33 |
| Bi(1)′ | 2.36 | 2.89 | 2.63 | 2.50 | 2.39 | 2.33 | 3.14 | 3.12 | 3.18 | 3.13 | 3.10 | 3.11 | 2.33 |
| Bi(2) | 2.84 | 2.93 | 2.98 | 2.84 | 2.84 | 2.95 | 3.06 | 3.07 | 3.07 | 3.19 | 3.23 | 3.03 | 3.20 |
| Bi(2)′ | 2.84 | 2.93 | 2.98 | 2.84 | 2.84 | 2.73 | 3.06 | 3.07 | 3.06 | 2.95 | 2.91 | 3.02 | 3.20 |
| Ti(1) | 4.45 | 4.49 | 4.19 | 4.45 | 4.35 | 4.44 | 4.24 | 4.24 | 4.14 | 4.14 | 4.14 | 4.20 | 4.45 |
| Ti(2) | 4.27 | 4.26 | 4.12 | 4.15 | 4.26 | 4.25 | 4.11 | 3.99 | 3.93 | 3.91 | 3.88 | 4.32 | 4.29 |
| Ti(2)′ | 4.27 | 4.26 | 4.12 | 4.15 | 4.26 | 4.30 | 4.11 | 3.99 | 4.03 | 4.06 | 4.09 | 4.35 | 4.29 |
| O(1) | 1.94 | 2.03 | 1.93 | 1.94 | 1.92 | 1.94 | 2.02 | 2.02 | 1.97 | 1.97 | 1.95 | 1.96 | 2.05 |
| O(1)′ | 1.94 | 2.03 | 1.93 | 1.94 | 1.92 | 1.94 | 2.02 | 2.02 | 2.03 | 2.02 | 2.04 | 1.99 | 2.05 |
| O(2) | 2.28 | 2.31 | 2.30 | 2.29 | 2.28 | 2.28 | 2.33 | 2.33 | 2.33 | 2.34 | 2.36 | 2.30 | 2.33 |
| O(2)′ | 2.28 | 2.31 | 2.30 | 2.29 | 2.28 | 2.28 | 2.33 | 2.33 | 2.33 | 2.31 | 2.30 | 2.30 | 2.33 |
| O(3) | 1.72 | 1.99 | 1.82 | 1.72 | 1.72 | 1.72 | 2.04 | 2.04 | 2.04 | 2.04 | 2.04 | 2.04 | 1.89 |
| O(3)′ | 1.72 | 1.99 | 1.82 | 1.72 | 1.72 | 1.74 | 2.04 | 2.04 | 2.04 | 2.04 | 2.04 | 2.04 | 1.89 |
| O(4) | 1.73 | 1.79 | 1.78 | 1.73 | 1.73 | 1.67 | 1.83 | 1.83 | 1.83 | 1.78 | 1.79 | 1.84 | 1.63 |
| O(4)′ | 1.73 | 1.79 | 1.78 | 1.73 | 1.73 | 1.79 | 1.83 | 1.83 | 1.83 | 1.88 | 1.87 | 1.87 | 1.63 |
| O(5) | 2.01 | 2.10 | 2.06 | 2.02 | 2.01 | 2.01 | 2.21 | 2.04 | 2.03 | 2.03 | 2.03 | 2.16 | 2.18 |
| O(5)′ | 2.01 | 2.10 | 2.06 | 2.02 | 2.01 | 2.01 | 2.21 | 2.04 | 2.07 | 2.07 | 2.06 | 2.16 | 2.18 |
| O(6) | 2.01 | 2.10 | 1.95 | 2.02 | 2.01 | 2.01 | 2.01 | 2.05 | 2.05 | 2.04 | 2.04 | 2.29 | 1.96 |
| O(6)′ | 2.01 | 2.10 | 1.95 | 2.02 | 2.01 | 2.01 | 2.01 | 2.05 | 2.04 | 2.05 | 2.05 | 2.25 | 1.96 |
| $\Sigma V_{total}$ | 0.30 | 0.20 | 0.19 | 0.26 | 0.28 | 0.30 | 0.16 | 0.14 | 0.14 | 0.15 | 0.15 | 0.20 | 0.32 |
| $\Sigma V_{corr}$ | 0.30 | 0.17 | 0.17 | 0.25 | 0.29 | 0.30 | 0.12 | 0.09 | 0.08 | 0.09 | 0.11 | 0.18 | 0.31 |

[a] Calculated AVs and $\Sigma V$s for the underlying *Fmmm* parent structure of $Bi_4Ti_3O_{12}$ (under the column labeled PAR), for the underlying *Fmmm* parent structure in combination with each of the *F2mm*, *Bmab*, *Bbab*, *Bbam*, and *Fmm2* modes individually (under the columns labeled *F2mm*, *Bmab*, *Bbab*, *Bbam*, and *Fmm2*, respectively) and in combination with the first two of these modes, the first three of these modes etc. (under the columns labeled 2 modes, 3 modes, . . . , 5 modes). Calculated AVs and $\Sigma V$s are also given for the correct $R = 1.8\%$ structure refinement, for an $R = 2.7\%$ false minimum structure, and for the original structure refinement of Dorrian *et al.* $\Sigma V_{total}$ includes all atoms in the asymmetric unit whereas $\Sigma V_{corr.}$ excludes oxygen atoms bonded to Bi in the $Bi_2O_2$ layers.

for the previous structure refinement of Dorrian *et al.* (*10*) (see under the column headed Dorrian).

The first point to make is that the bond valence method clearly distinguishes between the correct crystal structure and those resulting from false minima in the refinement process (see the $\Sigma$Vs under the columns headed 2.7% and Dorrian). Reliable crystal structure refinements usually give calculated valences that are in accord with theoretical valences to within $\pm 0.1$–$0.2$ valence units (see the examples given in Refs. (*14–16*)), unless the compound contains distortions that arise from steric or electronic effects. In the final refined crystal structure of $Bi_4Ti_3O_{12}$ (listed in the column headed 1.8%) the apparent valences are all largely in accord with theoretical valences except for the oxygens bonded to the Bi atoms of the $Bi_2O_2$ layers. The apparent over- and underbonding of these oxygens is, however, a consistent feature among the three independently rerefined structures as well as for other structure types containing this structural unit (see Section 3.3). Given this consistency, we conclude that the apparent over- and underbonding of the oxygens bonded to the Bi atoms of the $Bi_2O_2$ layers is normal for this type of structural unit and is due to a stereoactive lone pair on the Bi atoms of the $Bi_2O_2$ layers. For this reason we have listed $\Sigma$Vs for the various modes and structures both including and excluding these oxygen atoms. A more detailed discussion of this point is given in Section 3.3.

Returning to Table IV, it can be seen that the underlying *Fmmm* parent structure is characterized by a strong underbonding of the Bi cations in the perovskite *A* site (i.e. Bi(1), Bi(1)′)) as well as of the apical O(3), O(3)′ oxygen anions, by a strong overbonding of the Ti cations in the perovskite *B* sites (Ti(1), Ti(2), Ti(2)′) and by equatorial oxygen anions (O(1), O(1)′, O(5), O(5)′, O(6), O(6)′) which are satisfactorily bonded. An identical pattern recurs for $Bi_3TiNbO_9$. $Bi_2WO_6$ is somewhat of a special case in that there are now no perovskite *A* sites nor sites equivalent to the apical O(3), O(3)′ oxygen anions of $Bi_4Ti_3O_{12}$. Nevertheless, the apparent overbonding of the perovskite *B* cations as well as the apparently satisfactory bonding of the equatorial oxygen anions (see Table V) is still present in the calculated AVs of the parent structure (*8*).

In trying to understand why these materials need to lower their symmetry to satisfy bonding requirements, it is necessary to consider why the mixture of over-, under-, and satisfactory bonding cannot be remedied by non-symmetry-destroying measures such as a change in unit cell dimensions or in $z$ fractional coordinates. Simple alteration of cell dimensions cannot satisfy bonding requirements in the case where some atoms are underbonded and some overbonded. For example, in $Bi_4Ti_3O_{12}$, change of unit cell dimensions without any change in fractional coordinates cannot simultaneously increase the AV of the Bi atoms in the perovskite *A* sites (i.e., Bi(1), Bi(1)′) as well as decrease the AV of the Ti atoms in the perovskite *B* sites (Ti(1), Ti(2), Ti(2)′). However, it is less obvious that the effect of changing $z$ coordinates consistent with *Fmmm* symmetry cannot satisfy bonding requirements. In the parent *Fmmm* structure modifying the $z$ coordinate of one atom to improve its AV invariably worsens the AV of another. For example, changing the $z$ fractional coordinates of the Ti(2), Ti(2)′ perovskite *B* cations such that they are placed in the center of their surrounding $O_6$ octahedra might improve the AV of the apical O(3), O(3)′ oxygen atoms but it worsens the AV of the apical O(4), O(4)′ oxygen atoms. Clearly, within the constraints of *Fmmm* symmetry, the bonding requirements of all atoms cannot be satisfied simultaneously.

The question now arises as to the crystal chemical reasons underlying the presence

TABLE V

CALCULATED AVs AND $\Sigma V$s FOR THE PARENT AND REFINED STRUCTURES OF $Bi_4Ti_3O_{12}$, $Bi_3TiNbO_9$, $Bi_2WO_6$, AND $Bi_2(Sr_{0.9}Ba_{0.1})Ta_2O_9$. EQUIVALENT ATOMS OCCUR IN THE SAME ROWS

| $Bi_4Ti_3O_{12}$ *B1a1* | | | $Bi_3TiNbO_9$ *A2₁am* | | | $Bi_2(Sr_{0.9}Ba_{0.1})Ta_2O_9$ *A2₁am* | | | $Bi_2WO_6$ *P2₁ab* | | |
|---|---|---|---|---|---|---|---|---|---|---|---|
| Atom | Parent | Final | Atom | Parent | Final | Atom | Parent | Final | Atom | Parent | Final |
| Bi(1) | 2.36 | 3.21 | Bi(1) | 2.24 | 3.00 | $Sr_{0.9}Ba_{0.1}$ | 2.14 | 3.64 | | | |
| Bi(1′) | 2.36 | 3.10 | | | | | | | | | |
| Bi(2) | 2.84 | 3.23 | Bi(2) | 2.86 | 3.07 | Bi(1) | 2.83 | 3.11 | Bi(1) | 2.79 | 3.18 |
| Bi(2′) | 2.84 | 2.91 | | | | | | | Bi(1′) | 2.79 | 3.16 |
| Ti(1) | 4.45 | 4.14 | | | | | | | W(1) | 6.46 | 6.06 |
| Ti(2) | 4.27 | 3.88 | Ti,Nb | 4.85 | 4.44 | Ta | 5.68 | 5.18 | | | |
| Ti(2′) | 4.27 | 4.09 | | | | | | | | | |
| O(1) | 1.94 | 1.95 | | | | | | | O(1) | 1.98 | 2.11 |
| O(1′) | 1.94 | 2.04 | | | | | | | O(1′) | 1.98 | 1.95 |
| O(2) | 2.28 | 2.36 | O(3) | 2.30 | 2.33 | O(3) | 2.39 | 2.46 | O(2) | 2.23 | 2.31 |
| O(2′) | 2.28 | 2.30 | | | | | | | O(2′) | 2.23 | 2.31 |
| O(3) | 1.72 | 2.04 | O(1) | 1.53 | 1.94 | O(1) | 1.82 | 2.07 | | | |
| O(3′) | 1.72 | 2.04 | | | | | | | | | |
| O(4) | 1.73 | 1.79 | O(2) | 1.68 | 1.77 | O(2) | 1.85 | 1.72 | O(3) | 1.81 | 1.86 |
| O(4′) | 1.73 | 1.87 | | | | | | | O(3′) | 1.81 | 1.85 |
| O(5) | 2.01 | 2.03 | O(4) | 2.04 | 1.97 | O(4) | 2.22 | 2.26 | | | |
| O(5′) | 2.01 | 2.06 | | | | | | | | | |
| O(6) | 2.01 | 2.04 | O(5) | 2.04 | 1.98 | O(5) | 2.22 | 2.12 | | | |
| O(6′) | 2.01 | 2.05 | | | | | | | | | 0.19 |
| $\Sigma V_{total}$ | 0.30 | 0.16 | $\Sigma V_{total}$ | 0.32 | 0.16 | $\Sigma V_{total}$ | 0.34 | 0.30 | $\Sigma V_{total}$ | 0.23 | 0.12 |
| $\Sigma V_{corr}$ | 0.30 | 0.11 | $\Sigma V_{corr}$ | 0.33 | 0.05 | $\Sigma V_{corr}$ | 0.35 | 0.26 | $\Sigma V_{corr}$ | 0.25 | |

and magnitude of the various observed displacive modes. Of the seven displacive modes compatible with *B*1*a*1 symmetry, only four (*F*2*mm*, *Bmab*, *Bbab*, and *Bbab*) entail sizeable atomic shifts (see Table 9 of (*6*)). A fifth (*Fmm*2), although involving only very small atomic shifts, is known to be present due to the existence of a small component of spontaneous polarization along the **c** direction. The remaining two modes (*F*12/*m*1 and *Bmam*) refine to give such small atomic shifts that they have been neglected. The effect upon the $\Sigma$Vs of the individual addition of each of these five modes to the *Fmmm* parent structure is shown in Table IV under the columns headed *F*2*mm*, *Bmab*, *Bbab*, *Bbam*, and *Fmm*2, respectively, and is illustrated graphically in Fig. 5.

Clearly AVs are most strongly affected by the *F*2*mm* and *Bmab* displacive modes. To first order, the major effects of the ferroelectric *F*2*mm* displacive mode are to largely remedy the strong underbonding of the Bi atoms in the perovskite A sites as well as the underbonding of the apical O(3), O(3)′ oxygen atoms. Not surprisingly, it has virtually no effect upon the overbonded Ti atoms. This requires an octahedral rotation mode such as the *Bmab* mode in which $TiO_6$ octahedra rotate about an axis parallel to the polar **a** direction (see Fig. 2 of Ref. (*6*)). Its effects include a reduction of the overbonding of the Ti atoms and an increase in the AVs of the Bi atoms. The effect upon the AVs of adding both the *F*2*mm* and the *Bmab* modes to the *Fmmm* parent structure is listed under the column headed "2 modes." Ignoring the apparent over- and underbonding of the O(2), O(2)′ and O(4), O(4)′ oxygen atoms, it can be seen that the major deficiencies remaining are a slight

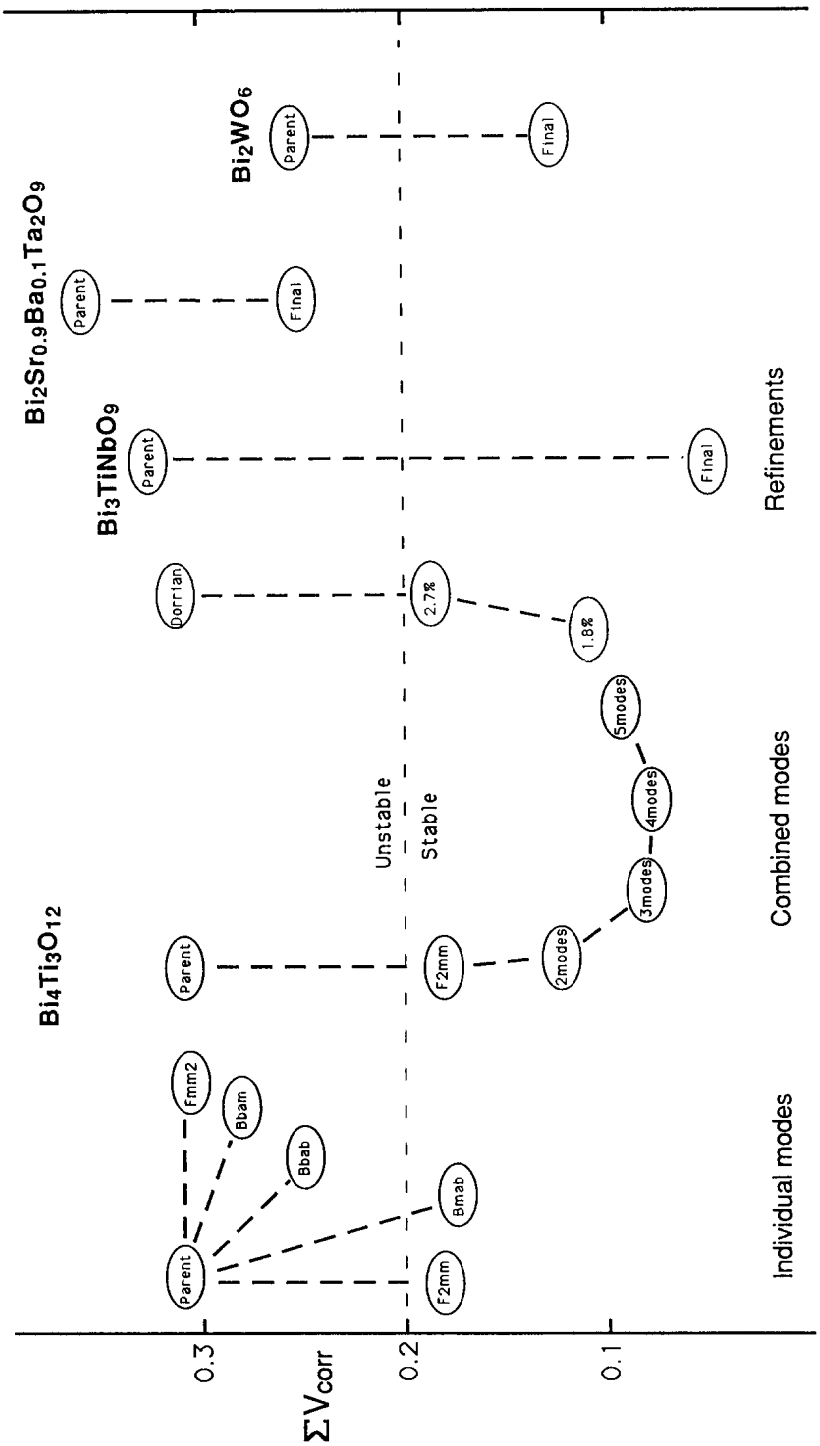


FIG. 5. Schematic illustration of $\Sigma V_{corr}$, the root mean square deviation of the $\Delta V$s (listed in Tables IV and V), for $Bi_4Ti_3O_{12}$, $Bi_3TiNbO_9$, $Bi_2Sr_{0.9}Ba_{0.1}Ta_2O_9$, and $Bi_2WO_6$. For $Bi_4Ti_3O_{12}$ the individual as well as the cumulative effect of the principal modes is shown. The $\Sigma V_{corr}$s for the parent and the refined structures for all the above compounds are also juxtaposed. The line at $\Sigma V = 0.2$ indicates the generally agreed threshold for stability.

overbonding of the Ti atoms and the O(5), O(5)′ oxygen atoms. The cumulative effect upon the ΣVs of each of these modes is also shown in Table IV and illustrated graphically in Fig. 5.

The presence of *F*2*mm* and *Bmab* displacive modes automatically implies the coexistence of a *Bbab* displacive mode corresponding to rotations of $TiO_6$ octahedra about the *c*-axis. Antimirror symmetry perpendicular to **c**, however, constrains the central $Ti(1)O_6$ octahedron not to rotate and the outer $Ti(2)O_6$ and $Ti(2)'O_6$ octahedra to rotate in the opposite sense. The rotation of the $Ti(2)O_6$ octahedron refined for this mode is shown in Fig. 4 of Ref. (*6*) and in Fig. 4. As might be expected, the principal effect is to reduce the AVs of the Ti(2) and Ti(2)′ atoms (via a slight increase in size of the $Ti(2)O_6$ and $Ti(2)'O_6$ octahedra) but not the AV of the Ti(1) atom. Rotation of the central $Ti(1)O_6$ octahedron about **c** requires a mode of *Bbam* symmetry. The structural reason underlying the observed large rotation angles for these modes (the angular rotations are +7.5°, 0°, −7.5° for the *Bbab* mode and 1.7°, 6.5°, 1.7° for the *Bbam* mode) thus appears to be the need to reduce still further the AV of the Ti atoms. The coexistence of *Bbab* and *Bbam* modes then automatically induces the small amplitude *Fmm*2 displacements responsible for the small component of spontaneous polarization along the **c** direction, but the amplitude of this mode is such that is has minimal effect upon the calculated AVs (see the column headed *Fmm*2 in Table IV and also Fig. 5). The very small amplitude *F*12/*m*1 and *Bmam* modes similarly would appear to be induced and also have minimal effect upon the AVs.

The above discussion provides a reasonably coherent view of the crystal chemistry of $Bi_4Ti_3O_{12}$. While one should be wary of making sweeping generalizations, it nonetheless seems clear that the fundamental reason for the large contribution to the calculated spontaneous polarization due to the rigid motion along **a** of the $(Ti_3O_{10})^{2-}$ part of the perovskite slabs relative to the [001] strings of Bi atoms is the strong underbonding in the unmodulated *Fmmm* parent structure of the Bi atoms in the perovskite *A* sites. Such a statement also holds true for $Bi_3TiNbO_9$. The case of $Bi_2WO_6$ ($n = 1$) is somewhat special for the reasons given above and really needs to be considered separately. The corresponding strong overbonding of the Ti atoms in the perovskite B sites similarly will induce the observed large amplitude octahedral rotation modes, i.e., *Bmab*, *Bbab*, and *Bbam*. The question of the relative amplitudes of these various modes, however, is a delicate compromise dependent upon the relative degrees of over- and underbonding of the various cations and anions making up the underlying parent structure.

### *3.2 Application to Other Aurivillius Phases*

The bond valence approach has also been applied to the rerefined structures of $Bi_3TiNbO_9$ and $Bi_2WO_6$ (see Refs. (*7*, *8*)). Again this approach differentiates between the correct crystal structures and those resulting from false minima in the refinement process. The picture that emerges for $Bi_3TiNbO_9$ is very similar to that given above. For $Bi_2WO_6$, the picture is not quite so clearcut. Table V shows calculated AVs and ΣVs for both the underlying *Fmmm* parent structures and the final refined structures of $Bi_4Ti_3O_{12}$, $Bi_3TiNbO_9$, and $Bi_2WO_6$. Calculated AVs and ΣVs are also given for both the underlying *Fmmm* parent structure and the reported structure of $Bi_2(Sr_{0.9}Ba_{0.1})Ta_2O_9$ (the only other member of this family whose structure has been reported—see (*17*)). Equivalent atoms in the structures are listed in the same rows to enable comparisons to be made. It is notable in this latter

case that the AV of the perovskite *A* site cation ($Sr_{0.9}Ba_{0.1}$) is apparently already satisfactorily bonded in the parent structure. Note the high AVs of this perovskite *A* site cation and the equatorial O(4) anion for the reported structure. A rerefinement of this crystal structure is in progress. For each of the above three structures, ΣVs are also included in Fig. 5.

### *3.3 Oxygen Atoms Bonded to Bi in the $Bi_2O_2$ Layers*

In the $Bi_4Ti_3O_{12}$ structure refinement Bi(2) and Bi(2)′ occupy very anisotropic sixfold sites (ninefold if bonds >3 Å are considered) between a layer of O(2), O(2)′ on one side and a layer of O(4), O(4)′ on the other, and show satisfactory AVs. However, O(2) and O(2)′ occupy regular tetrahedral sites between adjacent layers of Bi(2), Bi(2)′, respectively, and appear to be significantly overbonded. Conversely, O(4), O(4)′, which complete the sixfold coordination polyhedra for Bi(2), Bi(2)′, appear to be significantly underbonded. This overbonding and underbonding of O(2), O(2)′ and O(4), O(4)′, respectively, in the case of $Bi_4Ti_3O_{12}$, are common features of equivalent O atoms in all the Aurivillius phases whose structures have been redetermined (see Table V). Furthermore, this same feature is observed in BiOF (*18*), which contains the same $Bi_2O_2$ structural unit as occurs in the Aurvillius phases. Using an $r_0$ of 1.993 Å for $Bi^{3+}$–$F^-$ derived from $BiF_3$ (*19*), the apparent valences for BiOF are Bi = 3.01, O = 2.41, F = 0.60. Similarly, the isomorphous $Pb_2O_2$ layer in red PbO (*20*) gives an apparent valence for O of 2.30, using an $r_0$ of 2.112 for $Pb^{2+}$–$O^{2-}$. The AV for the tetrahedrally coordinated O atom in all these compounds is consistently 10–20% high, and yet the structural unit $Bi_2O_2$ ($Pb_2O_2$ in red PbO) in no way appears to be frustrated. If it were, a *c*-axis expansion could readily provide a decrease in AV for this atom.

Andersson and colleagues (*21–23*) have given a plausible explanation of such phenomena and of the structure of such materials in terms of a stereoactive lone pair ($Bi^{3+}$–lone pair distance of ~0.98 Å) on the Bi cations pointing along the **c** direction away from the layer of tetrahedrally coordinated O anions. A $Bi^{3+}$–lone pair distance of ~0.98 Å distance corresponds almost exactly to the difference in *c*-axis height of the Bi(2) cation and the O(4) anion in $Bi_4Ti_3O_{12}$. The nonbonded interaction between this stereochemically active lone pair and the neighboring oxygen anions is then understood to be the reason why the $Bi_2O_2$ layer does not move closer to the top of the perovskite slab and hence increase the AVs of the apparently underbonded Bi(2) and O(4) atoms. It might reasonably be asked why Bi(2) should be stereochemically active whereas the Bi cation in the perovskite *A* site appears to show no such steric effect. The two sites, however, are in quite distinct bonding environments. Bi(2) is bonded quite anisotropically, whereas Bi(1) is in a high coordination, cuboctahedral bonding environment. Kepert (*24*) has shown that increasing coordination number forces lone pairs closer to the central atom and reduces their influence on the stereochemistry until, for very large coordination numbers, the nonbonding pair of electrons has virtually no influence on the stereochemistry.

We therefore propose that the calculated AVs for the O(2), O(2)′ oxygen atoms (i.e. >2 or apparently overbonded) and the O(4),O(4)′ oxygen atoms (i.e. <2 or apparently underbonded) represent satisfactory bonding for this portion of the $Bi_4Ti_3O_{12}$ structure and for the equivalent portions of the $Bi_3TiNbO_9$ and $Bi_2WO_6$ structures. This applies to the equivalent oxygen atoms in all the Aurivillius phases, and other structures containing the same $Bi_2O_2$ structural unit such as BiO*X*,*X* = halide. Thus we believe that ΣVs calculated excluding these oxygen atoms give a more reliable indication of the plausibility of the refined structures.

### *3.4 Properties Understood in Bond Valence Terms*

From consideration of apparent valences calculated for the *Fmmm* parent structures of the Aurivillius phases, the large spontaneous polarizations observed along **a** ($P_x$) in $Bi_4Ti_3O_{12}$ and $Bi_3TiNbO_9$ can be largely attributed to the gross underbonding of $Bi^{3+}$ in the perovskite *A* site. The partial or complete replacement of $Bi^{3+}$ ($r_0$ = 2.094 Å) in the perovskite *A* site by $Ba^{2+}$ ($r_0$ = 2.285 Å), $Sr^{2+}$ ($r_0$ = 2.118 Å), or $Pb^{2+}$ ($r_0$ = 2.112 Å) (as, for example, in the $n$ = 2 family $Bi_2BaTa_2O_9$, $Bi_2BaNb_2O_9$, $Bi_2SrTa_2O_9$, $Bi_2SrNb_2O_9$, etc.) is known to have the effect of lowering the magnitude of the spontaneous polarization, the Curie temperature $T_c$, and the size of the orthorhombic distortion (*25*). This can be understood in bond valence terms as follows. Substitution of the above divalent cations for $Bi^{3+}$ in the A site of the parent structure approximately satisfies their bonding requirements (see Table V) and thereby reduces or eliminates much of the driving force for the *F2mm* mode (responsible for the large spontaneous polarization). Overbonding of the perovskite B site, however, remains, and hence so do the *Bmab* and *Bbab* octahedral rotation modes responsible for the $\sqrt{2}a_p \times \sqrt{2}a_p$ doubling of the basal plane cell.

It was previously believed that the overwhelmingly dominant contribution to ferroelectricity in $Bi_4Ti_3O_{12}$ ($n$ = 3), $Bi_3TiNbO_9$ ($n$ = 2), and $Bi_2WO_6$ ($n$ = 1) was due to the displacement of the octahedral cations (W, Ti, Nb) away from the center of their surrounding octahedron of oxygen atoms (*5*). The new structure refinements of $Bi_4Ti_3O_{12}$ (*6*), $Bi_3TiNbO_9$ (*7*), and $Bi_2WO_6$ (*8*), however, show that this is not the case. Rather, the major component of the large spontaneous polarization is due to the large *a*-axis displacements of the $Bi^{3+}$ ions in the perovskite *A* sites with respect to the chains of corner-connected $TiO_6$ octahedra, or vice-versa, as shown in Fig. 2. There is still a contribution to $P_x$ arising from a displacement of the perovskite *B* cation away from the center of its surrounding octahedron of oxygen atoms but this is by no means the dominant contribution even in the case of $Bi_2WO_6$ (see Table III). Thus, by virtue of apparent valence calculations, we now have a new insight into the structural origin of ferroelectricity in $Bi_4Ti_3O_{12}$, $Bi_3TiNbO_9$, and $Bi_2WO_6$.

## 4. Conclusion

In the present work we have endeavored to understand the structural origin of ferroelectricity in the displacive ferroelectric $Bi_4Ti_3O_{12}$ in crystal chemical terms. By using a modulated structure approach to describe the refined crystal structure of this compound, it has been possible to recognize how each of the observed displacive modes contributes to the satisfaction of the bonding requirements of each of the atoms. Some modes have a more dramatic effect than others. The *a*-axis polarization, the major ferroelectric component, appears to result from gross underbonding of the perovskite *A* atom in the undistorted parent structure. The much smaller *c*-axis component of spontaneous polarization is induced by the need to compensate for residual overbonding of Ti(1), Ti(2), and Ti(2)′ by coexisting *Bbab* and *Bbam* modes.

While one should be wary of overinterpretation of bond valence calculations, this present work demonstrates their ability to distinguish between similar models. AV and $\Sigma V$ calculations were able to show the inadequacy of the $R$ = 2.7% false minimum refinement with respect to the correct $R$ = 1.8% refinement as shown in Fig. 5. Also, when comparing equivalent structural units in related compounds, such as $Bi_4Ti_3O_{12}$, $Bi_3TiNbO_9$, and $Bi_2WO_6$, the calculations can be interpreted more fully. Finally, as the structural basis for ferroelectricity in these three members of the bismuth titanate fam-

ily has been previously misunderstood, as a result of incorrect structure refinements, much of the physical data collected for these materials will need to be reinterpreted.

## References


1. B. Aurivillius, *Arkiv. Kemi.* **1,** 463 (1949).
2. B. Aurivillius, *Arkiv. Kemi.* **2,** 519 (1951).
3. E. C. Subbarao, *Ferroelectrics* **5,** 267 (1973).
4. K. Singh, D. K. Bopardikar, and D. V. Atkare, *Ferroelectrics* **82,** 55 (1988).
5. R. E. Newnham, R. W. Wolfe, and J. F. Dorrian, *Mater. Res. Bull.* **6,** 1029 (1971).
6. A. D. Rae, J. G. Thompson, R. L. Withers, and A. C. Willis, *Acta Crystallogr. B.* **46,** 474 (1990).
7. J. G. Thompson, A. D. Rae, R. L. Withers, and D. C. Craig, *Acta Crystallogr. B.*, **47,** 174 (1991).
8. A. D. Rae, J. G. Thompson, and R. L. Withers, to be published.
9. C. J. Bradley and A. P. Cracknell, "The Mathematical Theory of Symmetry in Solids," pp. 146–161, Clarendon Press, Oxford (1972).
10. J. F. Dorrian, R. E. Newnham, D. K. Smith, and M. I. Kay, *Ferroelectrics* **3,** 17 (1971).
11. R. W. Wolfe, R. E. Newnham, D. K. Smith, and M. I. Kay, *Ferroelectrics* **3,** 1 (1971).
12. R. W. Wolfe, R. E. Newnham, and M. I. Kay, *Solid State Commun.* **7,** 1797 (1969).
13. I. D. Brown and D. Altermatt, *Acta Crystallogr. B.* **41,** 244 (1985).
14. I. D. Brown, *Chem. Soc. Rev.* **7,** 359 (1978).
15. M. O'Keeffe, *Struct. Bonding* **71,** 161 (1989).
16. I. D. Brown, *in* "Structure and Bonding in Crystals" (M. O'Keeffe and A. Navrotsky, Eds.), Vol. 2, pp. 1–30, Academic Press, New York (1981).
17. R. W. Wolfe, R. E. Newnham, R. S. Horsey, and F. A. Diaz, *Mater. Res. Bull.* **8,** 1183 (1973).
18. J. L. Soubeyroux, S. F. Matar, J. M. Reau, and P. M. Hagenmuller, *Solid State Ionics* **14,** 337 (1984).
19. O. Greis and M. Martinez-Ripoll, *Z. Anorg. Allg. Chem.* **436,** 105 (1977).
20. P. Boher, P. Garnier, J. R. Gavarri and A. W. Hewat, *J. Solid State Chem.* **57,** 343 (1985).
21. S. Andersson and S. Åstrom, *Natl. Bur. Standards, 5th Mat. Symp.*, 3 (1972).
22. J. Galy, G. Meunier, S. Andersson, and S. Åstrom, *J. Solid State Chem.* **9,** 92 (1975).
23. B. G. Hyde and S. Andersson, "Inorganic Crystal Structures," Ch. 10, Wiley–Interscience, New York (1989).
24. D. L. Kepert, "Inorganic Stereochemistry," Springer-Verlag, Berlin (1982).
25. E. C. Subbarao, *J. Phys. Chem. Solids* **23,** 665 (1962).